

## 2.5 Precision QCD at Large $Q^2$

QCD, the theory of the strong interaction, is the least precisely tested component of the Standard Model. High statistics data samples at the Tevatron Collider combined with increasingly sophisticated higher order perturbative QCD calculations not only provide stringent tests of perturbative QCD, but do so at distance scales which extend down to 0.1 milli fermi. This is an order of magnitude smaller than the weak scale, and the smallest distance currently probed in experimental particle physics. It is therefore quite plausible that new physics beyond the Standard Model associated with a new interaction at very small distance scales would first manifest itself as a deviation from QCD predictions at the Tevatron Collider.

The present focus of QCD analyses in CDF goes beyond the traditional comparison of observed distributions to leading-order (LO) or next-to-leading-order (NLO) QCD predictions. CDF measurements of the Drell-Yan cross-section and of the asymmetry in W production and decay have already been used to constrain parameterizations of parton densities. It is expected that Run II data samples will enable the explicit extraction of the fundamental parameters of the theory ( $\alpha_S$  and the parton distributions) in several different processes. The agreement or disagreement between these measured parameters and the corresponding measurements from other experiments at lower  $Q^2$  provides a rigorous test of QCD in the same way that different measurements of  $\sin^2 \theta_W$  tests the electroweak sector of the standard model.

The luminosity upgrades to the Tevatron for Run II will extend the sensitivity of studies of QCD into a substantially higher energy regime where new high- $Q^2$  phenomena may be found. In addition, new calculations, higher statistics, and improvements in the understanding of detector performance will increase the precision and scope of the present tests of QCD. To illustrate the extended region that will be probed by the upgrade, the following topics will be discussed along with the discovery potential in each channel: a) jet cross section, b) direct photons, c) W and Z boson production, d) multijet events, and e) the extraction of  $\alpha_S$  and the parton densities. These analyses in Run II will rely upon the plug upgrade to extend high quality jet measurements to  $|\eta| < 3.0$ , the SVX II to provide high efficiency b-tagging, and the high rate DAQ system to collect very high statistics data

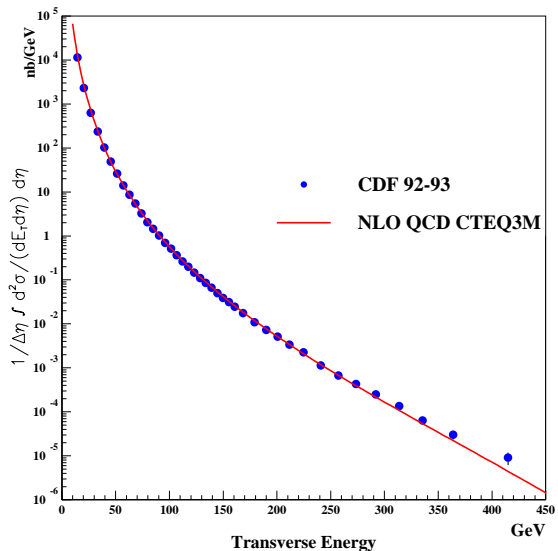


Figure 2.41: The inclusive jet cross section measured by the CDF detector compared to the NLO QCD prediction.

samples.

### 2.5.1 Jet Cross Section

Recently the inclusive jet cross section ( $p\bar{p} \rightarrow \text{jet} + X$ ) has been calculated[1] to order  $\alpha_s^3$ . This calculation greatly reduces the theoretical uncertainty associated with choice of renormalization scale. Figure 2.41 shows, as a function of jet  $E_t$ , the jet cross section measured by CDF, based on an integrated luminosity of  $21 \text{ pb}^{-1}$ . The cross-section has been measured over a range  $\approx 9$  orders of magnitude. The solid line in Figure 2.41 is the prediction of NLO QCD. This provides a remarkably good description of the data except for the highest  $E_t$  jets. A more detailed comparison of the data to NLO QCD is shown in Figure 2.42 where  $(\text{data} - \text{theory})/\text{theory}$  is plotted on a linear scale. The data from Run Ia ( $21 \text{ pb}^{-1}$ ) is plotted as the open circles and preliminary results from Run Ib ( $87 \text{ pb}^{-1}$ ) as the solid circles. The data sets are statistically consistent and show an excess of observed jets over theory for jet  $E_t$  above 250 GeV. The deviations could indicate (i) the need for corrections to the perturbative QCD calculations that go beyond NLO, (ii) modifications of the parton distribution functions, or (iii) something new beyond the standard model. Measurements using higher statistics data samples are clearly needed in the  $E_t$  range

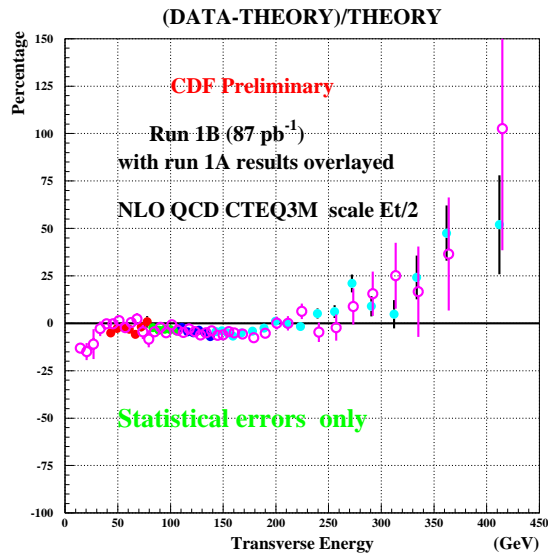


Figure 2.42: Comparison of the observed inclusive jet cross section measured by the CDF detector with the prediction of next to leading order QCD. The comparison shows  $(\text{data} - \text{theory})/\text{theory}$  as a function of jet transverse energy. The open circles are Run Ia data, solid circles Run Ib.

above 300 GeV where there are only 308 jets from the Run I data set. Extrapolating to an expected  $2 \text{ fb}^{-1}$  for Run II, we would measure about 6000 jets with  $E_t > 300 \text{ GeV}$  and extend the measurement shown in Figure 2.42 to a jet  $E_t$  of about 500 GeV.

Two other distributions which provide additional sensitive tests of perturbative QCD at small distance scales are the two-jet mass distribution (Fig. 2.43) and the distribution of total transverse energies (summed over all jets in the event) shown in Fig. 2.44. Preliminary measurements of both these distributions also show an excess of events at large di-jet mass and sum  $E_t$ . As for the inclusive jets, the region of deviation from the QCD prediction will be explored in much more detail with the factor of 20 statistical improvement expected in Run II.

High statistics data samples from Run II will improve the ability to test QCD at sufficiently small distances to search for new physics beyond the standard model. Quark substructure would give rise to an increase in jet production at large transverse energy. This property can be incorporated into the QCD Lagrangian by adding a short range contact term with an effective distance scale defined by the parameter  $\Lambda_C$  [2]. Figure 2.45 shows the theoretical prediction

for the high energy end of the inclusive jet cross section. The solid curves are the ratios of the cross sections with a compositeness scale  $\Lambda_C$  to the cross section predicted by QCD with no compositeness. Also shown is the ratio of the measured inclusive jet cross section from  $21 \text{ pb}^{-1}$  of data to the QCD prediction. Measuring this jet spectrum from  $2 \text{ fb}^{-1}$  will decrease the statistical errors shown in Figure 2.45 by a factor of about 10. This would yield a sensitivity that corresponds to a  $\Lambda_C$  value in the range 1.8 to 2.0 TeV. In addition to providing a sensitive search for new small-distance interactions, the shape of the spectrum at transverse energies as large as 500 GeV will be sensitive to soft gluon resummation effects associated with the approaching kinematic limit at high  $E_t$ , and therefore provide an important test of resummation techniques [8]. The measured inclusive jet spectrum would also tie down the high  $x$  end of the parton distribution functions. The Tevatron measurement at high  $x$  will eventually be very valuable when compared to LHC measurements in order to understand if the excess is due to parton distribution functions or some new effective interaction.

The two-jet invariant mass spectrum is sensitive to heavy objects produced with a strong coupling. In chiral color models[3], a massive octet of gluons is predicted which would lead to a broad (axigluon) resonance in the two-jet invariant mass spectrum. This resonance, because of its strong coupling, would produce a sizable enhancement in the di-jet mass spectrum above the QCD background. The two-jet mass spectrum from approximately  $106 \text{ pb}^{-1}$  of data is consistent with a smooth (nonresonant) distribution. This excludes axigluons in the mass range  $200 \leq M_a \leq 1000 \text{ GeV}$ . A data sample of  $2 \text{ fb}^{-1}$  should extend the search for axigluon contribution up to a mass limit of 1.2 TeV. Other models also predict resonant enhancements in the dijet mass spectrum. Current CDF limits on ability to distinguish between model are summarized in Fig. 2.46. The sensitivity achieved by analyses of the di-jet mass spectrum is clearly competitive with other searches based on the worlds data. A data sample of  $2 \text{ fb}^{-1}$  will extend the range of di-jet mass that can be examined by about 200 GeV.

Finally, the NLO calculations (order  $\alpha_s^3$ ) have the additional feature that the jet cross section depends on the effective radius in the  $\eta$ - $\phi$  metric used for clustering. Comparing these predictions to data will permit a more detailed investigation of the relationship

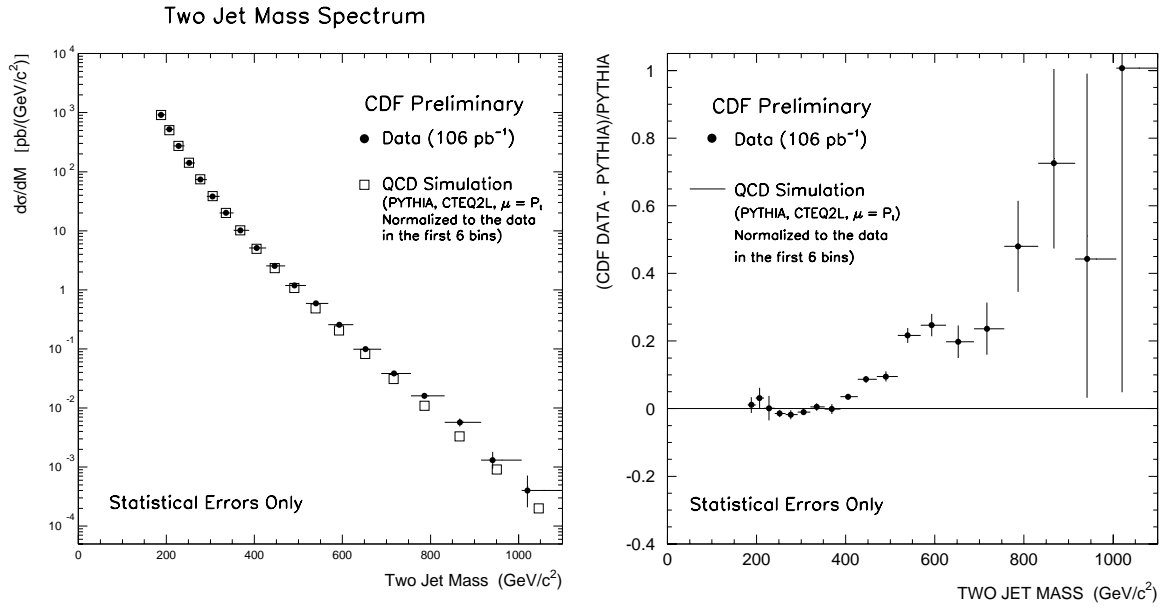


Figure 2.43: Left: Two-jet mass distribution compared to LO QCD simulation. Right: Two jet invariant mass spectrum compared to LO QCD predictions in terms of  $(\text{data-theory})/\text{theory}$ .

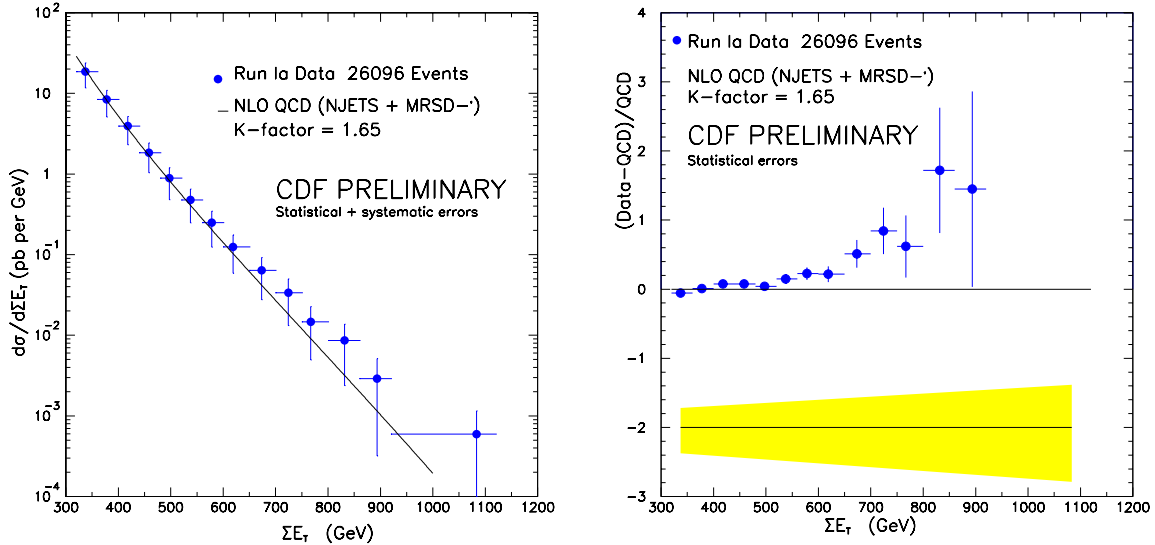


Figure 2.44: Left: Total transverse energy distribution compared to a NLO QCD prediction. Right: The same comparison in terms of  $(\text{data} - \text{theory})/\text{theory}$ .

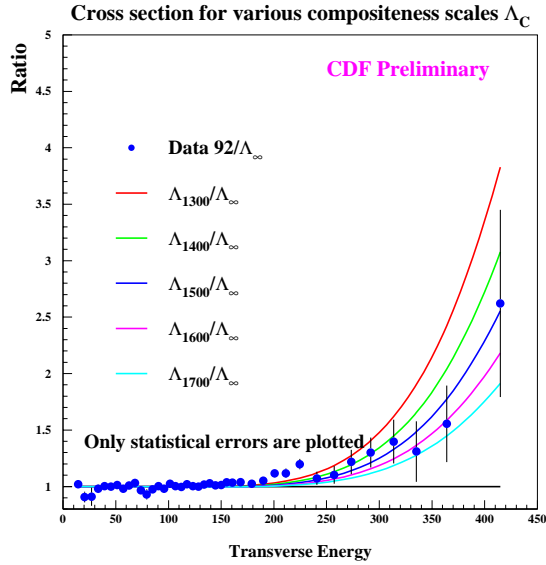


Figure 2.45: The ratios of inclusive jet cross sections with compositeness scales  $\Lambda_C$  to the QCD prediction with no compositeness. Also shown is the ratio of data/QCD prediction for 21 pb<sup>-1</sup> of data from Run Ia (solid points).

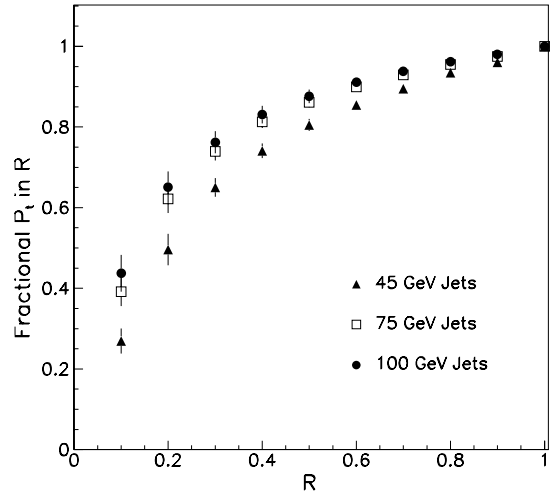


Figure 2.47: The variation in jet size with  $E_t$  as measured by the fractional  $P_t$  of tracks within a cone of radius  $R$ .

between hadronic jets and the underlying scattered partons, and in particular enable a detailed study of jet merging and sharing of energy between two nearby jets. As shown from Figure 2.47 the jet size narrows with increasing  $E_t$  as measured from the fractional  $P_t$  of tracks within a jet cone of radius  $R$ . Understanding these features of jets is necessary for precise measurements of the properties of particles decaying to jets, for example the top quark and a possible light Higgs bosons.

### Excluded Mass Regions for New Particles

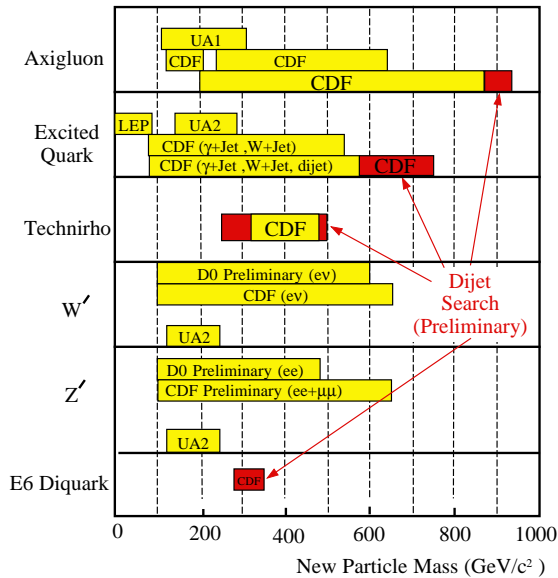


Figure 2.46: CDF limits resulting from the absence of a dijet resonance in the observed two-jet mass spectrum, compared with the worlds limits.

### 2.5.2 Multijet Events

The study of events with three or more jets in the final state provides a test of perturbative QCD that complements the inclusive jet and two-jet measurements. A comparison of recent CDF measurements of the mass dependent jet multiplicity distributions (Fig. 2.48) shows that LO QCD predictions give a reasonable description of the measurements. However, at the highest energies, both the statistical uncertainties on the measurements and the systematic uncertainties on the predictions are large. With a 2 fb<sup>-1</sup> data sample the statistical uncertainties on the data points will shrink by more than a factor of 5. Improvements in computing resources will be needed to provide corresponding improvements in the statistical uncertainties on parton shower Monte Carlo predictions. Furthermore, the availability of a

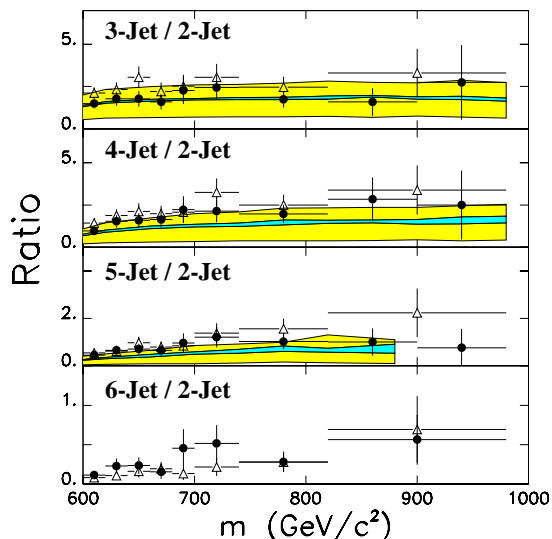


Figure 2.48: CDF measured ratios of N-jet to 2-jet events shown as a function of multijet mass (points) for jets with  $E_t > 20$  GeV, compared to LO QCD predictions from a matrix element calculation (bands) and from the HERWIG parton shower Monte Carlo program (open triangles).

NLO three-jet calculation together with further understanding of the theoretical uncertainties based on analyses of current data samples may well result in substantial reductions in the estimates of these uncertainties. Hence it is likely that the precision of quantitative comparisons between predicted and observed multijet properties will improve by about a factor of 5.

### 2.5.3 Direct Photons

Studies of direct photon production in CDF complement jet studies, and have the advantage that photon energies are measured with greater precision than the energies of jets. So far direct photons have provided the best experimental and theoretical probe of low  $x$  parton distributions and QCD at the Tevatron. The current measurements indicate the presence of a source of photon transverse momentum in addition to that calculated from NLO QCD, as illustrated in figure 2.49. The normal QCD prediction falls below the data at low  $p_t$ , while the addition of the parton shower matches the data quite well. This has implications for any hadron collision measurement using NLO QCD. It is also clear from this plot that the increased luminosities will help this measurement sta-

tistically at high  $p_t$ .

Direct photon + jet angular distributions are interesting due to the quark propagator, as opposed to jet production with its gluon propagators. This is shown in the right part of figure 2.49, where the dijet, W+jet and photon+jet angular distributions are shown along with their NLO QCD predictions. One sees the dramatic differences between jets and photon/W production. Further studies of the photon+jet measurement as well as photon + 2 jets will probe the direct photon production mechanisms.

### 2.5.4 W and Z boson production

The data collected at the Tevatron Collider during Run I should provide 100,000  $p\bar{p} \rightarrow W + X$  and 10,000  $p\bar{p} \rightarrow Z + X$  events after all selection cuts (including both electron and muon W/Z decays). Figure 2.50 shows the  $W(Z)$  cross sections as a function of the number of associated jets in the event using  $107 \text{ pb}^{-1}$  of electron decays from Run I. 20% of these events have associated QCD jets, with approximately 1% having 3 or more jets (jet  $E_t > 15$  GeV). An extrapolation to a  $2 \text{ fb}^{-1}$  data sample from Run II yields, for example, 1.9 million W bosons, including approximately 380,000 with associated jets. These data can be used for a variety of important tests of the Standard Model, for top quark studies and to search for new phenomena. A brief discussion of the potential for these measurements is given below, based upon the assumption of a  $2 \text{ fb}^{-1}$  data sample from Run II. It is important to note that the high rate DAQ system available for Run II will record all available W/Z triggers onto tape.

The hadronic production of W and Z bosons provides the opportunity to test the Standard Model in processes where the parton level scattering is identified by the presence of the bosons and which naturally occur at a high  $Q^2$  scale. Measurements of  $\alpha_s$  can be extracted from jet multiplicity spectra. The data shown in Fig. 2.50 would be increased by a factor of about 40 in Run II. This would allow measurements of the jet multiplicity associated with W bosons out to six jets. A complementary measurement of  $\alpha_s$  can be obtained from W and Z  $P_t$  spectra of the type shown in Figure 2.51. Recently, calculations have been performed at order  $\alpha_s^2$  for the  $P_t$  spectra of the W/Z.[5] These calculations reduce the theoretical uncertainty in the cross section. With  $2 \text{ fb}^{-1}$  of data, the  $P_t$  reach for W's would allow a significant

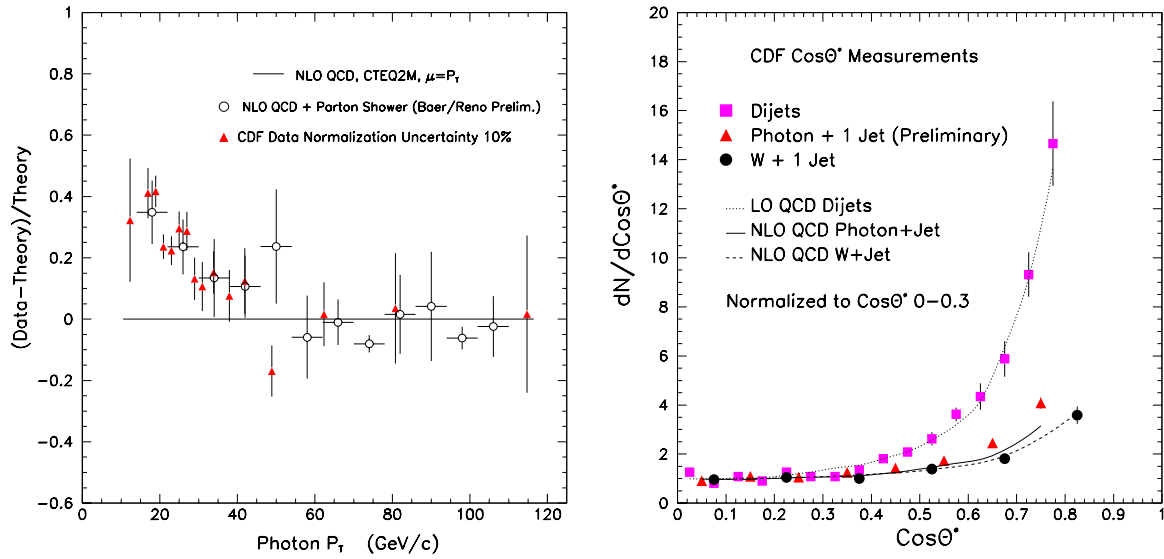


Figure 2.49: Left: Comparison of the direct photon differential cross-section with NLO QCD predictions. Right: Photon, W boson and di-jet angular distributions

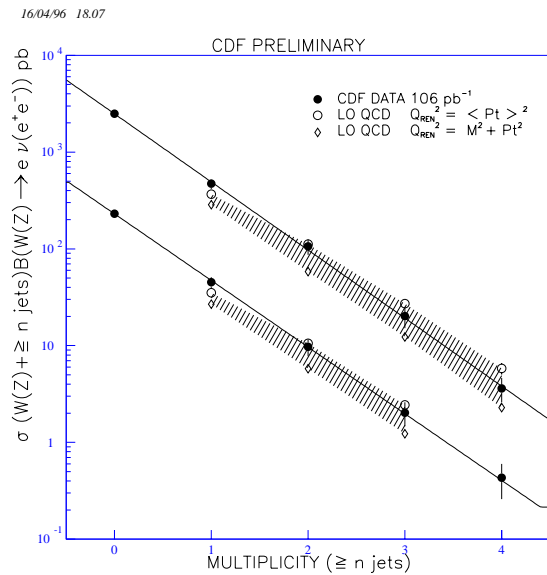


Figure 2.50:  $W(Z) + \geq n$  jets cross sections compared with the QCD LO predictions.

measurement out to 250 GeV. The  $Z P_t$  spectrum can be measured with very low background. The Run II data sample would be 40 times larger than that shown in Figure 2.51, providing about 200,000 Z bosons. The low  $P_t$  part of the W and Z spectra provide data useful for a measurement of gluon resummation effects. Non-standard processes, such as a techni-rho would appear as an enhancement in the  $P_t$  spectrum.[4]

A critical analysis of the direct production of W and Z bosons with QCD jets can be made from the 380,000 W+jet and 38,000 Z+jet events expected from  $2 \text{ fb}^{-1}$  of data. Figures 2.51 through 2.53 illustrate measurements made from a sample of data ( $73 \text{ pb}^{-1}$ ) from the current Tevatron run. The  $E_t$  distribution of the highest energy jet from W + 1 and 2 jet events is plotted in Fig. 2.52. The W-jet and Z-jet invariant mass distributions are shown in Figure 2.51. In all these Figures the data (points) are compared to LO QCD calculations (histogram). A 50 fold increase in the statistics (electron plus muon decay channels) shown in these plots (electron decays only) will allow a study of the QCD jet spectra out to  $E_t$  of about 250 GeV. Currently NLO predictions are available only for W/Z + 1 jet events, but calculations for higher multiplicities should be available for comparison to the Run II data.

A careful study of direct W and Z boson production with jets is important both for an accurate mea-

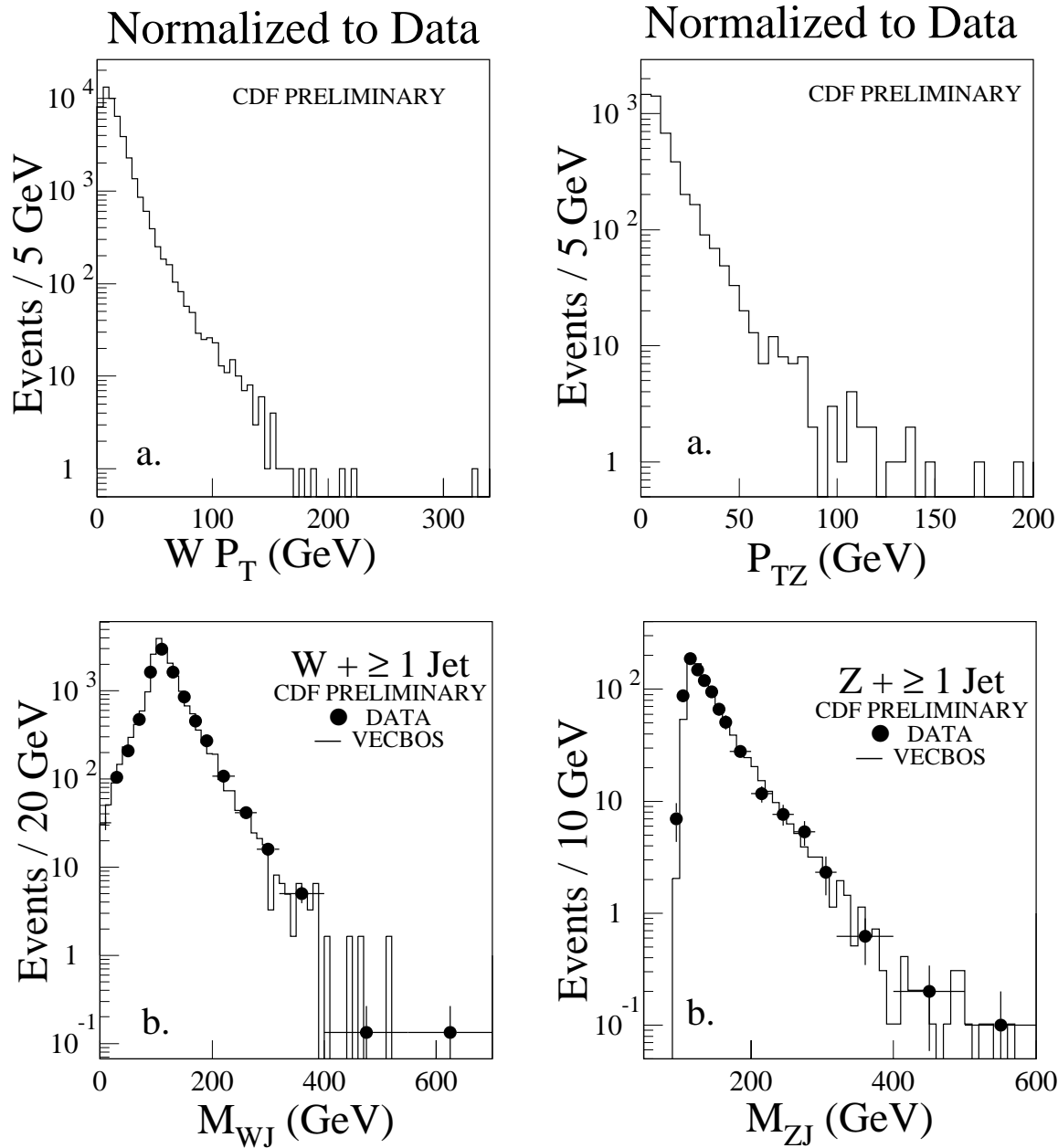


Figure 2.51: Top left: The W transverse momentum distribution from  $73 \text{ pb}^{-1}$  of Run I data. Bottom left: The invariant mass distribution of the W boson and the highest energy jet. Top right: The Z transverse momentum distribution from  $73 \text{ pb}^{-1}$  of Run I data. Bottom right: The invariant mass distribution of the Z boson and the highest energy jet

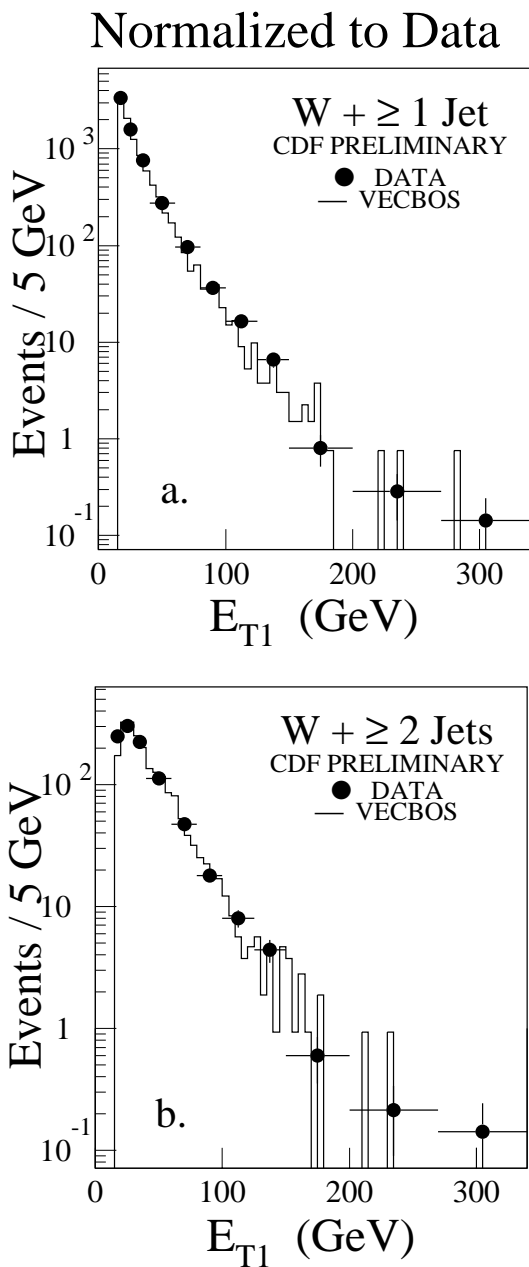


Figure 2.52: The jet  $E_{T1}$  spectra for events with a)  $W + \geq 1$  jet, and b)  $W + \geq 2$  jets.

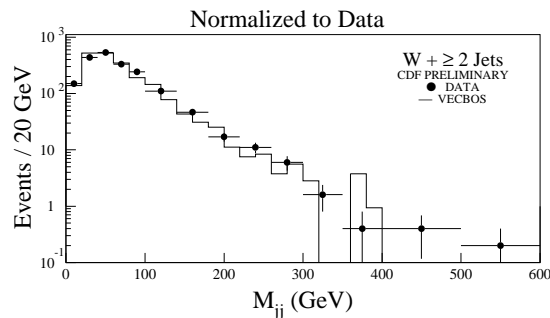


Figure 2.53: a) The invariant mass of the two highest- $E_T$  jets.

surement of the top mass and in searches for new particles which decay to  $W/Z$ 's or are produced in association with them. Processes involving technicolor-type models could produce heavy particles decaying into  $W$  pairs. The exact nature of such couplings are not certain, but do provide some impetus to examine the potential discovery limits. From different scenarios, and depending on the coupling, it may be possible to detect techni-rho's with masses up to 250 GeV. Backgrounds for Higgs bosons can be reduced by searching for production in channels with associated  $W/Z$  bosons. The jet-jet invariant mass spectrum from events with  $W$  bosons is shown in Fig. 2.53 for a sample of Run I data. The data (points) are well reproduced by a leading order QCD calculation out to jet-jet masses of 300 GeV. Scaling this up to a  $2 \text{ fb}^{-1}$  data sample predicts on the order of 600  $W$  events with a di-jet in the invariant mass range from 260 to 300  $\text{GeV}/c^2$ . This provides the background to any new particle with mass in this range decaying to dijets and produced in association with a  $W$  boson. The high statistics  $W/Z + \text{jet}$  sample available in Run II should permit a good understanding of the normal QCD production and allow a search for new particles out to masses of 300  $\text{GeV}/c^2$ .

### 2.5.5 The extraction of $\alpha_S$ and the parton densities

An important goal of QCD analyses of CDF data in the near future is the extraction of  $\alpha_S$  and/or the parton densities from all processes for which there are reasonable data samples and reliable predictions. Some examples are the inclusive jet differential cross-section, the two-jet mass and angular dis-

tributions, jet and photon rapidity distributions, the charge asymmetry in leptonic W decays, the direct photon differential cross-section, jet multiplicity distributions, and the W, Z, and Drell-Yan transverse momentum distributions. These measurements will provide new constraints on the parameters of the theory. The self consistency of the extracted parameters, together with their consistency with measurements from other experiments at lower energies and  $Q^2$ -scales, provides a rigorous test of perturbative QCD.

The published CDF inclusive jet differential cross-section has been used to extract  $\alpha_S$  ([7]). Preliminary results are shown in Fig. 2.54. These are not only consistent and competitive with the worlds knowledge of  $\alpha_S$ , but also demonstrate in a single measurement the running of the strong coupling "constant". The real strength of the measurements of  $\alpha_S$  based on the CDF jet spectrum is that these measurements probe the behaviour of the QCD coupling at high  $Q^2$ , extending the  $Q^2$  range of the worlds data by more than a factor of 4. With a data sample of  $2 fb^{-1}$  the statistical errors will shrink by a factor of 10 with respect to those shown in the figure, and the measurement will extend out to a  $Q^2$  of about  $(500 GeV)^2$ . In addition a  $2 fb^{-1}$  data sample would facilitate a precise simultaneous determination of  $\alpha_S$  and the parton distributions, which will enable systematic uncertainties associated with global structure function fits to be minimized. This is important since the global fit systematic uncertainties are difficult to quantify.

Reliable QCD predictions require a precise knowledge of the parton distributions. CDF Drell-Yan and W lepton charge asymmetry measurements are already being used to constrain these distribution functions. For example the current W asymmetry measurements are shown in Fig. 2.55 for a data sample of about  $70 pb^{-1}$ . Hence, for a  $2 fb^{-1}$  data sample the statistical uncertainties will shrink by a factor of 5, and provide a very interesting constraint on the parton distributions.

### 2.5.6 Summary of the benefits of Tevatron Run II to QCD studies

The QCD studies described in this section will be greatly extended through the combination of the very large data samples expected in Run II and complementary improvements of the CDF II detector described in this TDR. The new plug calorimeter will permit high quality jet measurements out to

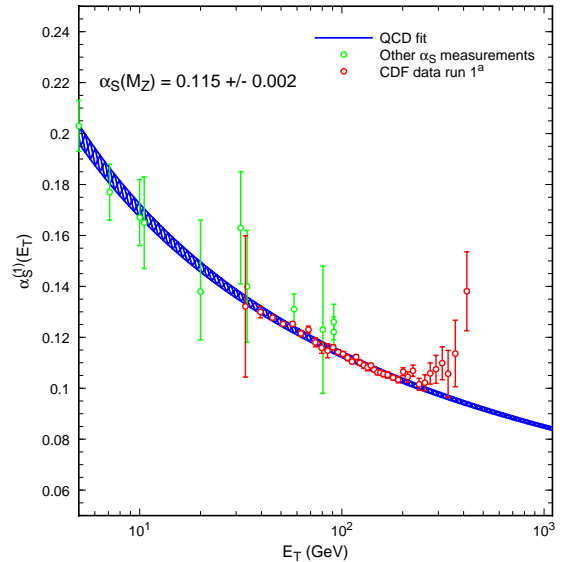


Figure 2.54: The value of  $\alpha_S(E_T)$  extracted by Giele and Glover using published CDF data.

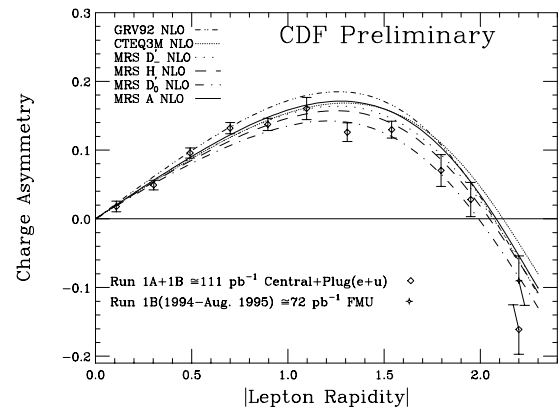


Figure 2.55: The lepton charge asymmetry measured in W decays.

$|\eta| < 3.0$ , thus extending measurements to a region of phase space where resummation effects could be tested. Tagging jets containing a b hadron decay with the SVX II permits a clean study of top quarks, a sensitive search for light Higgs bosons, and searches for other new particles. Clearly most of the QCD studies will profit from the potential of a factor of 20 increased statistics in Run II. To take advantage of this in terms of data recorded, the upgraded DAQ system is essential.

Table 2.11 shows the events expected in some selected channels from a Run II exposure of  $2 fb^{-1}$ , based upon extrapolations from Run I data already analyzed.

Table 2.11: QCD events expected from a  $2 fb^{-1}$  Run II data sample

Production Channel	Events
jet ( $j$ ) + X, $ \eta  \leq 1.0, E_T \geq 300$ GeV	$6.4 \times 10^3$
$jj$ + X, $M_{jj} \geq 600$ GeV	$3.0 \times 10^4$
$\gamma$ + X, $p_T(\gamma) \geq 25$ GeV	$6.0 \times 10^6$
$\gamma\gamma$ + X, $p_T(\gamma_1, \gamma_2) \geq 12$ GeV	$1.4 \times 10^4$
$Z + \geq 1j$ , $E_T(j) \geq 100$ GeV	$1.0 \times 10^3$
$W + \geq 1j$ , $E_T(j) \geq 100$ GeV	$1.0 \times 10^4$

To take full advantage of these data the systematic errors associated with jet measurements will have to be reduced by making internal consistency checks on the data. For example the high statistics Z+jet and photon+jet data samples will permit balancing precisely measured electromagnetic calorimeter energy (a photon or Z boson) against jet calorimeter energy. With reduced systematic errors, these data have the potential for testing QCD down to length scales of about 0.1 milli fermi. The running of  $\alpha_S$  can be measured in detail in a  $Q^2$  range from about  $(30 GeV)^2$  to  $(500 GeV)^2$ , and parton distribution functions measured with high precision. In total these data have the potential for making stringent tests of the QCD sector of the Standard Model and hopefully revealing a deeper understanding of elementary particle physics.

# Bibliography

- [1] S. Ellis, Z. Kunszt and D. Soper, Phys. Rev. **D40** 2188 (1989); U. of Oregon Preprint OITS 436 (1990).
- [2] E. Eichten, K. Lane and M. Peskin, Phys. Rev. Lett. **50**, 811 (1983).
- [3] J. Bagger, C. Schmidt, S. King, Phys. Rev. **D37** 1188 (1988).
- [4] E. Eichten and K. Lane, Phys. Lett. **222** 274 (1989).
- [5] P. Arnold and M.H. Reno, FERMILAB-Pub-88/168 (1988).
- [6] Martins, Roberts and Stirling, Z. Phys. **C42**, 277 (1989).
- [7] W.T. Giele and E.W.N. Glover, Moriond 95.
- [8] S. Catani, M. Mangano, P. Nason and L. Trentadue, CERN-TH/96-86 hep-ph/9604351.